Motor Unit Sampling From Intramuscular Micro-Electrode Array Recordings

Agnese Grison, Jaime Ibáñez Pereda, and Dario Farina, *Fellow, IEEE*

***Abstract*— Recordings of electrical activity from muscles allow us to identify the activity of pools of spinal motor neurons that send the neural drive for muscle activation. Decoding motor unit and motor neuron activity from muscle recordings can be performed by high-density (HD) electrode systems, both non-invasively (surface, HD-sEMG) and invasively (intramuscular, HD-iEMG). HD-sEMG recordings are obtained by grids placed on the skin surface while HD-iEMG signals can be acquired by micro-electrode arrays. While it has been shown that HD-iEMG allows the accurate decoding of a larger number of motor units when compared to HD-sEMG, the dependence of motor unit yield on the parameters of the micro-electrode arrays is still unexplored. Here, we used recently developed HD-iEMG electrodes to record from hundreds of recording sites within the muscle. This allowed us to investigate the impact of electrode number, inter-electrode distance, and the number of muscle insertions on the ability to sample motor units within the muscle. Specifically, we recorded both HD-sEMG and HD-iEMG from the Tibialis Anterior muscle of two healthy subjects at various contraction intensities (10%, 30%, and 70% of maximum voluntary contraction, MVC). For the first time, we present intramuscular recordings with more than 140 electrodes inside a single muscle, achieved through multiple implants of high-density micro-electrode arrays. Through systematic offline analyses of these recordings, we tested different electrode configurations to identify optimal setups for accurately capturing motor unit activity. The results revealed that the density of electrodes in the micro-electrode arrays is the most critical factor for maximising the number of identified motor units and ensuring very high accuracy. Comparisons between intramuscular and surface recordings also confirmed that HD-iEMG consistently captures larger and more stable numbers of motor units across subjects and contraction levels. These results underscore the potential of HD-iEMG as a powerful tool for both clinical and research settings, particularly when precise motor unit decomposition is crucial.**

***Index Terms*— EMG, high-density, intramuscular, motor units.**

I. Introduction

RAPID advancements in neural interface technologies are fostering the development of innovative systems capable of restoring sensory, communicative, and control capabilities for individuals with impairments. These technologies enable interactions between the nervous system and external devices.

Myoneural interfaces utilising electromyography (EMG) to interface muscles offer a reliable and accessible means to capture motor commands issued by the central nervous system [1], [2]. By interfacing directly at the muscle level, these systems access the motor units, comprising spinal motor neurons and their innervated muscle fibers. The activity of motor units has been extensively studied over the past decades using intramuscular needles or wire electrode recordings [3], [4], [5].

To overcome the limited motor unit sampling offered by traditional needle or wire electrodes, high-density surface EMG (HD-sEMG) has been shown to enable the decoding of a significantly larger number of motor units [6], [7]. This has paved the way for the development of high-density intramuscular EMG (HD-iEMG) technologies [8], [9], which combine the selectivity of traditional intramuscular EMG with the extensive spatial sampling of high-density surface recordings. Indeed, HD-iEMG overcomes several limitations of traditional non-invasive muscle recordings to decompose motor neuron activity, such as the filtering effects of the volume conductor, sensitivity to electrode positioning [10], amplitude cancellation [11], and cross-talk [12], which often lead to reduced accuracy in estimating the neural drive to muscle. By providing greater spatial sampling and access to a larger pool of motor neurons, HD-iEMG enables a more precise and direct measurement of muscle activity. This advancement facilitates enhanced analysis of the multiple

Received 10 September 2024; revised 26 November 2024; accepted 13 January 2025. Date of publication 17 January 2025; date of current version 30 January 2025. The work of Agnese Grison was supported in part by U.K. Research and Innovation (UKRI) Centre for Doctoral Training in Artificial Intelligence (AI) for Healthcare under Grant EP/S023283/1 and in part by Huawei Technologies Research and Development (UK) Ltd. The work of Jaime Ibáñez Pereda was supported by project ECHOES (European Research Council (ERC) Starting) under Grant 101077693 and in part by the Consolidación Investigadora under Grant CNS2022-135366 funded by MCIN/AEI/10.13039/ 501100011033 and UE's NextGenerationEU/PRTR Funds. The work of Dario Farina was supported in part by NaturalBionicS (ERC Synergy) under Grant 810346 and in part by the Non-Invasive Single Neuron Electrical Monitoring (NISNEM Technology) [Engineering and Physical Sciences Research Council (EPSRC)] under Grant EP/T020970/1. *(Corresponding author: Dario Farina.)*

This work involved human subjects in its research. Approval of all ethical and experimental procedures and protocols was granted by the ethical board of Imperial College London ICREC under Application No. 19IC5640, and performed in line with the Declaration of Helsinki.

Agnese Grison and Dario Farina are with the Department of Bioengineering, Imperial College London, SW7 2AZ London, U.K. (e-mail: d.farina@imperial.ac.uk).

Jaime Ibáñez Pereda is with the Department of Bioengineering, Imperial College London, SW7 2AZ London, U.K., also with the BSICoS Group, the Aragón Institute of Engineering Research (I3A), and the Instituto de Investigación Sanitaria de Aragón (IIS Aragón), Universidad de Zaragoza, 50009 Zaragoza, Spain, and also with the Centro de Investigación Biomídica en Red en Bioingeniería, Biomateriales y Nanomedicina (CIBER-BBN), 50018 Zaragoza, Spain.

Digital Object Identifier 10.1109/TNSRE.2025.3531054

neural inputs that the motor neurons receive from different regions of the nervous system, offering a deeper understanding of the neural information underlying volitional motor control.

Recent advancements in intramuscular electrode technology have enabled EMG recordings with highly dense configurations [4], [8], allowing multi-channel recordings from dozens of detection sites within the muscle. Current HD-iEMG electrode designs have largely been informed by theoretical models, with limited empirical studies investigating the critical factors for optimal configuration in extracting motor unit information. As a result, the critical design parameters that maximise the ability of HD-iEMG to decode the neural signals driving muscle activity remain insufficiently explored.

In this study, we conducted experiments using newly developed HD-iEMG electrodes [4] to record muscle activity from the Tibialis Anterior muscle of two healthy participants at 10%, 30%, and 70% of the maximum voluntary contraction (MVC) during ankle dorsiflexion. We simulated different electrode configurations offline by selecting subsets of electrodes and analysing the number of decomposed units and the quality of the decomposition as outcome measures. This approach allowed us to evaluate the impact of key parameters, such as inter-electrode distance (IED), the number of recording sites, and the use of multiple HD-iEMG micro-electrode arrays within the same muscle, to maximise the decomposition potential of HD-iEMG.

In summary, this study made the following contributions:

1) We conducted, for the first time, intramuscular recordings with over 140 recording sites from a single muscle, marking the first instance of truly HD-iEMG;
2) We directly compared surface and intramuscular recordings from the same individuals under identical experimental conditions, assessing their respective capabilities in identifying motor unit populations;
3) We analysed the relative importance of inter-electrode distance and number of recording sites on motor unit sampling in intramuscular EMG.

II. Methods

A. EMG Model and Decomposition

A key challenge in EMG signal analysis is the deconvolution of the composite signals to isolate individual motor unit action potentials (MUAPs) and their firing sequences [13]. Mathematically, the EMG signal can be described by the following model:

$$\mathbf{x}(t) = \sum_{l=0}^{L-1} \mathbf{H}(l)\mathbf{s}(t-l) + \boldsymbol{\xi}(t) \tag{1}$$

Here, $\mathbf{x}(t) = [x_1(t), x_2(t), \ldots, x_M(t)]^T$ denotes the vector of M observed EMG signals, $\mathbf{s}(t) = [s_1(t), s_2(t), \ldots, s_N(t)]^T$ represents the N motor unit spike trains generating the EMG signals, and $\boldsymbol{\xi}(t)$ is the additive noise. The matrix $\mathbf{H}(l)$, with dimensions $M \times N$, contains the l^{th} sample of the MUAPs for the n^{th} motor unit and the m^{th} EMG channel.

This convolutional model is identical for HD-sEMG and HD-iEMG signals. The difference between the two recordings is the matrix $\mathbf{H}$ that defines the volume conductor. Therefore, the solution of the deconvolution problem is the same for the two recording modalities.

The convolutional model can be reformulated as an instantaneous mixture of an augmented vector of sources, comprising the N sources and their delayed versions. The extension factor L for the sources corresponds to the duration of the impulse response of the filter representing the volume conductor. The observations are also extended by R delayed versions in order to keep the ratio between the number of observations and the number of sources as high as possible. The instantaneous model can be written as:

$$\tilde{\mathbf{x}}(t) = \tilde{\mathbf{H}}\tilde{\mathbf{s}}(t) + \tilde{\boldsymbol{\xi}}(t) \tag{2}$$

where

$$\begin{aligned} \tilde{\boldsymbol{s}}(t) &= \left[\tilde{s}_1(t), \tilde{s}_2(t), \ldots, \tilde{s}_j(t), \ldots, \tilde{s}_N(t)\right]^T \\ \tilde{\boldsymbol{s}}_j(t) &= \left[s_j(t), s_j(t-1), \ldots, s_j(t-(L+R+1))\right] \end{aligned} \tag{3}$$

and $\tilde{\boldsymbol{H}}$ is constructed from the extended convolution kernels $\tilde{\boldsymbol{h}}$. The observed signal $\tilde{\boldsymbol{x}}(t)$ is:

$$\begin{aligned} \tilde{\boldsymbol{x}}(t) &= \left[\tilde{\boldsymbol{x}}_1(t), \tilde{\boldsymbol{x}}_2(t), \ldots, \tilde{\boldsymbol{x}}_i(t), \ldots, \tilde{\boldsymbol{x}}_M(t)\right]^T \\ \tilde{\boldsymbol{x}}_i(t) &= [x_i(t), x_i(t-1), \ldots, x_i(t-R)] \end{aligned} \tag{4}$$

The task then becomes determining the individual sources from the mixed signal.

Decomposition strategies for HD-EMG signals can be broadly categorised based on whether they utilise classic spike sorting methods (template matching) or blind source separation (BSS). Template matching approaches correlate the observed MUAP waveforms with predefined templates [14]. While effective under low-force conditions, these methods face challenges at medium to high-force levels [15] due to the increased recruitment of motor units. A large number of active motor units determines a high probability of MUAP superimpositions over time, making it difficult to separate individual MUAPs [14].

In contrast, BSS techniques, such as the convolution kernel compensation (CKC) [16] and its variants [17], [18], rely solely on the statistical properties of the motor unit discharge patterns for decomposition, ignoring filter kernel information [19]. These methods estimate the cross-correlation vector $\mathbf{c}_{s_n,\tilde{\mathbf{x}}} = E(s_n(t)\tilde{\mathbf{x}}(t))$ between the discharge pattern of the n^{th} motor unit and the observations, where $E(.)$ denotes mathematical expectation [18]. An empirically selected cost function is applied to each sample of the estimated discharge pattern $\hat{s}_n(t)$. The estimate $\hat{\mathbf{c}}_{s_n,\tilde{\mathbf{x}}}$ is iteratively updated using the following gradient-based rule [18]:

$$\hat{\mathbf{c}}_{\tilde{s}_n,\tilde{\mathbf{x}}} = \hat{\mathbf{c}}_{\tilde{s}_n,\tilde{\mathbf{x}}} + \eta(k)\frac{1}{T}\sum_n \frac{\partial F(\hat{\tilde{s}}_n(t))}{\partial \hat{\mathbf{c}}_{\tilde{s}_n,\tilde{\mathbf{x}}}}$$

$$\hat{\mathbf{c}}_{\tilde{s}_n,\tilde{\mathbf{x}}} = \frac{\hat{\mathbf{c}}_{\tilde{s}_n,\tilde{\mathbf{x}}}}{\|\hat{\mathbf{c}}_{\tilde{s}_n,\tilde{\mathbf{x}}}\|}$$

where $\eta(k)$ is the adaptive learning rate at iteration k.

Initially developed for HD-sEMG signal decomposition, these methods utilise cost functions F, such as $F(\tilde{s}) = 2 \cdot \text{atan}(\tilde{s}) - 2 \cdot \tilde{s} + \tilde{s} \cdot \log(1+\tilde{s}^2)$, to maximise source independence (or *sparseness*) while being robust to outliers [20].

Initially, BSS methods were developed and applied to HD-sEMG, as these techniques require a large number of recording channels. However, the advancement of HD-iEMG technologies has now enabled the use of BSS for intramuscular recordings as well. Recently, a novel BSS-based algorithm, Swarm-Contrastive Decomposition (SCD), was proposed specifically for HD-iEMG [21]. SCD utilises a particle swarm optimisation approach to adaptively traverse a polynomial family of nonlinearities. These nonlinearities are designed to approximate the asymmetric cumulants of the sources, which are statistical measures capturing the asymmetry and higher-order dependencies in the data.

The key innovation of SCD lies in its ability to tailor the nonlinearity to each source individually, allowing it to adapt more precisely to the characteristics of the data. By doing so, SCD can search the solution space more efficiently and effectively. It can also leverage data points that would typically be considered outliers, turning them into useful information for the decomposition process.

SCD has demonstrated superior accuracy and performance compared to other convolutive BSS techniques, for HD-iEMG data. In some instances, it has even surpassed the accuracy of manual decomposition methods, considered the gold standard in many applications [21]. Given these advantages, in this study we employed SCD for the signal decomposition of HD-iEMG data. For the decomposition of HD-sEMG data, we used the more commonly applied Convolutive Blind Source Separation (cBSS) technique [20]. In this way, we utilised the best algorithm for each type of data, acknowledging that SCD has not yet been validated for HD-sEMG data, hence our choice to use the validated cBSS method.

B. Data

The HD-iEMG signals were recorded using multi-channel micro-electrode arrays designed for acute recordings [4], [8]. Each micro-electrode array comprised 40 platinum detection points (140 μm $\times$ 40 μm) arranged in two linear arrays of 20 electrodes each, spaced by 1 mm. The two sides of the filament were shifted by 0.5 mm, resulting in a linear array with a 0.5 mm inter-electrode distance [4].

The HD-iEMG and HD-sEMG signals were recorded using a multi-channel amplifier (OT-Bioelettronica, Torino, Italy), sampled at 10,240 Hz, high-pass filtered at 10 Hz, and analog-to-digital converted with 16-bit resolution. The EMG signals were acquired in a monopolar derivation configuration, with a reference electrode placed on the ankle.

All experimental procedures adhered to the ethical guidelines set by Imperial College London (ICREC Project ID 19IC5640) and were performed in accordance with the Declaration of Helsinki, with informed consent obtained from all participants prior to each experiment.

Experiments were performed on the Tibialis Anterior muscle of two healthy men, aged 30 and 39 years. The participants had no history of neurological or musculoskeletal disorders. Although the sample size was small, the complexity of the recordings, involving multiple insertions into the same muscle, limited the feasibility of including a larger subject pool. Three intramuscular micro-electrode arrays were inserted into the TA of Subject 1 (S1), and four intramuscular micro-electrode arrays were inserted into the TA of Subject 2 (S2), approximately 3 cm apart in the longitudinal direction. An additional HD-iEMG array was inserted in the TA of S2 because of poor recording quality of one of the previously inserted arrays that had nearly half of the recording sites outside the muscle. Following insertion, subjects were asked about any discomfort caused by the HD-iEMG arrays at rest and during muscle contractions, and they reported none. Two 64-channel surface grids (4 mm IED, 13 $\times$ 5 configuration) were placed on the belly of the muscle, next to the intramuscular insertions for both subjects. Subjects were seated with their right leg and foot constrained to a dynamometer and instructed to sustain an isometric ankle dorsiflexion during all experiments. The participants completed an MVC trial after the insertion of the intramuscular electrodes, which helped secure the electrodes and provided a reference for measuring relative forces. The relative forces were determined as percentages of the MVC, with visual feedback provided to the subjects regarding the exerted force and target. The subjects performed trapezoidal contractions at 10, 30, and 70 %MVC ramping up and down at a rate of 10 %MVC/s. The force was sustained for 20 seconds at 10% and 30 %MVC, and for 10 seconds at 70 %MVC. These force levels were selected to encompass a range from low to medium to high intensity muscle contractions. The isometric portion of the contractions, corresponding to the plateau phase, was used for the decomposition to adhere to the stationary assumption of the model. All results are reported based on the isometric segments of the recordings, except for the recruitment threshold analysis. For this analysis, the separation filters of the decomposed motor units were reapplied to the entire contraction to track the motor units during the ramp [22]. After tracking, the discharge rates of each motor unit were recomputed during the plateau phase of the recording and utilized for the recruitment threshold analysis. Outliers, defined as values falling outside the interquartile range, were excluded as no manual cleaning was performed after tracking. The recruitment threshold was determined as the force level at which each motor unit began to fire regularly.

Figure 1 shows the setup of the electrodes for S1 (**i**) and for S2 (**ii**).

C. Experiments

Experiments were conducted to isolate specific variables and evaluate their impact on the yield and accuracy of motor unit identification from HD-iEMG recordings. Additionally, the yield and accuracy of decomposition from concurrently recorded HD-sEMG recordings are presented to provide a comparative analysis between the two types of recordings. The accuracy in decomposition was evaluated with the silhouette (SIL) measure, as defined in [20]. This metric is linearly associated to the accuracy with which the series of motor unit discharge times is estimated. To compare the accuracy of decomposition between HD-iEMG and HD-sEMG, we selected the top v units with the highest accuracy from the full set of HD-iEMG signals (i.e., 112 channels for S1 and 142 for S2), where v represents the number of units decomposed from the corresponding HD-sEMG. For example,

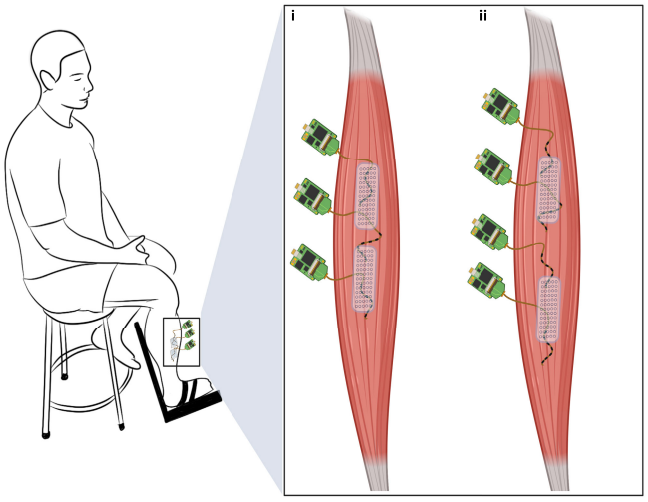

Fig. 1. Schematic representation of the experimental setup. HD-iEMG and HD-sEMG signals (2 grids, 64 channels with 4 mm IED) were concurrently recorded while participants were seated in a chair and were producing ankle dorsiflexions. **i** Three HD-iEMG electrodes were inserted in the TA of S1. **ii** Four HD-iEMG electrodes were inserted in the TA of S2. Created with BioRender.com.

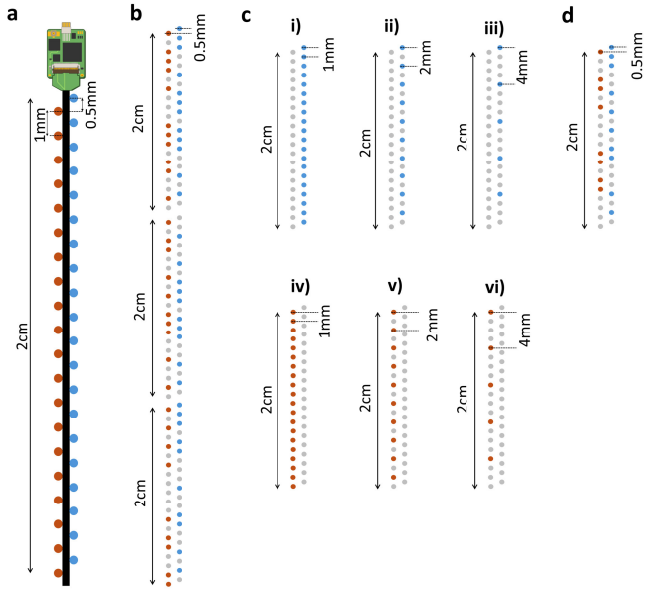

Fig. 2. The electrode array configurations considered in this study. **a** Schematic of electrode. **b** Representative example of the configuration for number of channels $q = 62$, and random selection $k = 1$. **c** Per electrode channel subsampling keeping a fixed IED. In detail: IED 1mm (**i**, **iv**), IED 2mm (**ii**, **v**), IED 4mm (**iii**, **vi**). **d** Schematic representation of the random subsampling implemented per electrode.

if the HD-sEMG decomposed 11 units at 10 %MVC for S1, we selected the top 11 units from the HD-iEMG decomposition and compared the distributions of the SILs.

For all subsequent analyses, channels that presented flat signal profiles or baseline noise exceeding three standard deviations the mean noise level were excluded from the study. Notably, approximately 15 channels from the third micro-electrode array in S2 were identified as external to the target muscle area. Consequently, the effective channel count was adjusted to 112 from an initial 120 for S1, and 142 from an initial 160 for S2. For the HD-sEMG analyses, 2 channels from S1 and 17 channels from S2 were excluded.

1) Data Analysis 1: This analysis aimed to study the accuracy and the number of decomposed motor units based on different numbers of available channels and their locations within the muscle. A subset of channels, denoted as p, was subjected to combinatorial assessment. Permutations were derived from the binomial coefficient $\binom{p}{q}$ for each of $q = 1, 2, 3, .., p$. This means that for each value of q, different combinations of q channels were selected from the total p channels. This process was repeated $k = 100$ times for each value of q to ensure robustness and reliability of the results. For subject S1, $p = 112$, and for subject S2, $p = 142$. Figure 2 **a** illustrates one such configuration for $q = 62$. This analysis was performed for all force levels (10, 30, 70 %MVC). Because the channels were always selected within the same micro-electrode arrays, changing the number of channels also corresponded to changing the density of electrodes.

2) Data Analysis 2: This analysis assessed the number of decomposed motor units by subsampling the channels for each electrode maintaining a fixed IED. Six configurations were tested per electrode. The electrode with 15 channels outside the muscle in S2 was excluded from this analysis. The configurations were as follows: IED 1 mm (**i**, **iv**), IED 2 mm (**ii**, **v**), IED 4 mm (**iii**, **vi**), as illustrated in Figure 2 **c**. Channels identified as flat or noisy in Experiment 1 were also excluded from this analysis. This occasionally resulted in fewer channels than the expected theoretical number.

To evaluate whether a stochastic selection of channels could yield comparable results to a systematic channel reduction, we compared these results with random subsampling of the channels. This analysis was conducted separately for each array, selecting k permutations based on the minimum number of available channels across all electrodes. This resulted in k=35 for S1, and k=36 for S2. Due to computational constraints, this analysis was performed only for 30 %MVC.

D. Hyperparameters

The decomposition process was executed on an AMD Rome processor paired with an Nvidia RTX 6000 GPU. In all experiments, only the selected channel configurations were varied. Signals were filtered with a high-pass filter with a cutoff frequency of 10 Hz. The low-pass filter cutoff was set at 4400 Hz for HD-iEMG and 500 Hz for HD-sEMG. Decompositions were conducted exclusively during isometric contractions, with the number of iterations capped at 250. For SCD applied to HD-iEMG, an extension factor of 20 was applied to the observations. The decomposition process was terminated if no new acceptable sources were identified for 20 consecutive iterations. For HD-sEMG decomposition, all parameters were chosen as specified in [20].

For all decompositions, the SIL cutoff was set at 0.85. In postprocessing, only units with a coefficient of variation of the interspike interval below 40% and firing rates lower than 30 Hz were retained for further analysis.

The level of agreement between the activities of motor units decoded from the surface and intramuscular recordings was

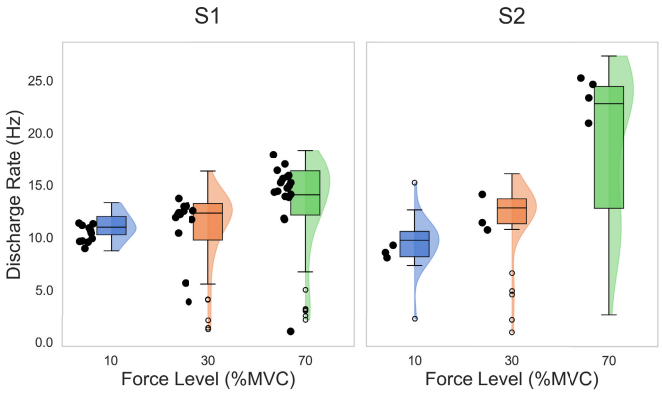

Fig. 3. Distribution of motor unit discharge rates (Hz) measured at three force levels (10%, 30%, and 70 %MVC) in two subjects (S1 and S2). The data combines measurements from two recording techniques: HD-iEMG (represented by boxplots with overlaid density plots in blue, orange, and green) and HD-sEMG (shown as black circles). The figure demonstrates how discharge rates generally increase with force level, with wider distributions observed at higher force levels. Each data point represents an individual motor unit's discharge rate, with the vertical axis showing rates from approximately 0-25 Hz.

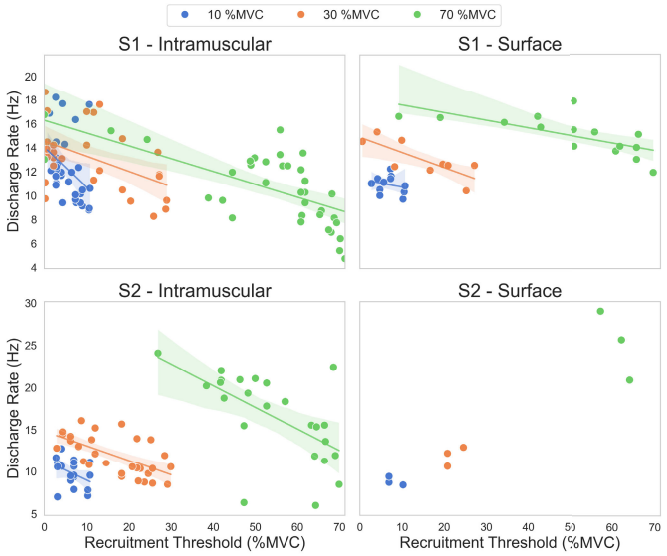

Fig. 4. Recruitment thresholds and motor unit discharge rates across the three force levels and the two subjects, and compared between motor units decomposed from the HD-iEMG and HD-sEMG signals. Relationship between motor unit recruitment thresholds (%MVC) and discharge rates (Hz) at three force levels (10%, 30%, and 70 %MVC) for two subjects (S1 and S2). Data are shown separately for intramuscular recordings (HD-iEMG, left panels) and surface recordings (HD-sEMG, right panels). Linear regression lines with 95% confidence intervals (shaded areas) demonstrate the negative correlation between recruitment threshold and discharge rate, particularly visible in the intramuscular recordings. Different force levels are color-coded (blue: 10%MVC, orange: 30%MVC, green: 70%MVC), showing distinct clusters of motor unit behaviour.

assessed using the Rate of Agreement (RoA). The RoA measures the fraction of commonly identified discharges relative to the total number of discharges, considering both common and not common firings. The RoA was therefore calculated as follows:

$$RoA = \frac{TP}{TP + FP_1 + FP_2}$$

In this equation, TP refers to the number of matched predicted activations within a deviation margin of ± 0.5 ms. FP_1 and FP_2 represent the counts of unmatched predicted activations, corresponding to firings present in only one of the two sets.

III. Results

A. Characterization of the Decomposed Motor Units

The number of motor units decomposed using HD-iEMG across the three force levels and the two subjects ranged between 24 and 53. With the HD-sEMG signals, the number of units decomposed was between 3 and 19. Table I summarizes the number of decomposed motor units from the maximum number of available channels per subject and contraction level. The distribution of discharge rates of all decomposed motor units is presented in Figure 3. Boxplots and density plots depict the distributions of motor units from HD-iEMG signals, while black circles indicate the values for the HD-sEMG signals. The discharge rates showed a consistent increase with force levels (Fig. 3 **a**), which is an expected outcome reflecting the physiological relationship between force production and neural drive. The values of the HD-sEMG closely align with the distributions of the HD-iEMG units, showing that similar information was extracted with both methods. Figure 4 shows the relationship between the recruitment threshold and the discharge rates. As expected, the firing rates increased relative to the excitatory input [23].

Additionally, Table I reports the number of matched units between the HD-iEMG and the HD-sEMG, and the RoA between them. This analysis provides a conservative estimate of the decomposition accuracy for the two recording types. Indeed, the RoA considers the total number of decomposition errors from the two methods. Importantly, we could find matched units between surface and intramuscular recordings in both subjects and at all contraction levels, with very high RoA, which provides a strong validation of the decomposition carried out with the two types of signals [20], [24]. The median SIL value of the matched units between the HD-iEMG and HD-sEMG signals was 0.94 (interquartile range: 0.93-0.97) for the HD-iEMG signals and 0.95 (interquartile range: 0.93-0.97) for the HD-sEMG signals. The slightly higher median SIL for HD-sEMG units likely reflects the fact that the matched units are predominantly superficial and so farther from the intramuscular electrodes, making them more difficult to decompose in HD-iEMG recordings.

B. Number of Decomposed Motor Units as a Function of the Number of Channels

Figure 5 illustrates an example of concurrently recorded signals at 70 %MVC for S1. Panel **a** shows the HD-iEMG signals and panel **c** shows the HD-sEMG signals. The respective raster plots are presented in panels **b** (HD-iEMG) and **d** (HD-sEMG). The intramuscular signals provide higher spatial specificity, with individual action potentials typically being detectable across 6-8 channels. As a consequence, HD-iEMG

TABLE I
NUMBER OF DECOMPOSED MOTOR UNITS FROM THE HD-IEMG AND THE HD-SEMG SIGNALS FOR S1 AND S2 AT DIFFERENT FORCE LEVELS. FOR EACH SUBJECT AND FORCE LEVEL, THE NUMBER OF COMMON MOTOR UNITS BETWEEN THE HD-IEMG AND THE HD-SEMG, TOGETHER WITH THE RANGE OF THEIR ROA, ARE PROVIDED

Subject	Force Level (%MVC)	No. of MUs (HD-iEMG)	No. of MUs (HD-sEMG)	No. of common MUs	RoA of common MUs
S1	10	40	11	4	89.3 - 100.0
	30	53	13	1	90.9
	70	52	19	3	87.9 - 96.4
S2	10	24	3	2	98.1 - 98.9
	30	45	3	1	97.4
	70	32	4	1	92.7

allowed a decomposition of a larger set of units than HD-sEMG (52 units vs 19 in this example).

Figure 6 displays the number of motor units decomposed as a function of the number of channels used. Results are presented separately for each subject and force level. Each data point represents the yield from a permutation of a channel subset (Fig. 2 **b**). The figure displays the relationship between the number of random channels and the number of identified motor units at 10 (blue), 30 (orange), and 70 %MVC (green). Each point on the graph represents one of the 100 permutations for each channel count. The solid lines on the graph indicate the average yield for a given channel count. The range of motor units decoded across different channel permutations was relatively broad. For example, in subject S1, using 80 channels, the number of decoded motor units varied between approximately 40 and 60. This substantial variation suggests that the precise location of the recording channels influences the decomposition yield, though it is not possible to determine the optimal placement of each recording site a priori.

The dashed lines in Fig. 6 represent the yield of motor units decomposed by HD-sEMG decomposition. The number of units is projected on the channel axis for HD-iEMG to indicate the number of channels needed on average by intramuscular recordings to match the motor unit yield of HD-sEMG based on 126 (S1) and 111 (S2) channels. Overall, HD-iEMG allowed the decomposition of a relatively large number of motor units across subjects. Notably, a strong reduction in units decomposed was observed when HD-sEMG data was used. For both subjects, decomposition of large sets of motor units (always above 20) was successfully achieved for all force levels using HD-iEMG.

C. Accuracy of Decomposition as a Function of the Number of Channels

Figure 7 **a** displays the mean SIL value of the motor units decomposed from each permutation run, for the HD-iEMG. As expected, SIL levels were generally higher at lower force levels [25] and for greater number of channels. The variability in SIL was greater with fewer channels, which is expected because fewer channels provide less information about each motor unit, making the decomposition process less reliable. In contrast, more channels provide a more robust filter, leading to a more accurate decomposition, as the same unit is observed across multiple channels. The SIL values began to plateau at around 80 channels for both subjects, suggesting that approximately 80 channels are necessary to achieve consistent and stable accuracy in decomposition.

TABLE II
NUMBER OF MOTOR UNITS DECOMPOSED FROM THE ELECTRODE CONFIGURATIONS PRESENTED IN FIG. 2 **c**, AVERAGED ACROSS IEDS

Subject	Force Level (%MVC)	IED 1 mm	IED 2 mm	IED 4 mm
S1	10	13.0 ± 7.4	10.5 ± 6.3	5.5 ± 3.1
	30	15.5 ± 13.0	7.3 ± 1.7	3.0 ± 2.1
	70	12.3 ± 8.8	5.5 ± 2.2	1.8 ± 1.3
S2	10	10.7 ± 4.8	8.8 ± 3.8	6.3 ± 1.0
	30	19.8 ± 5.8	9.0 ± 3.6	2.0 ± 1.1
	70	6.5 ± 3.2	1.3 ± 1.03	0

The decomposition quality was generally high, with SIL levels above the commonly used threshold value of 0.9. Figure 7 **b** presents the distribution of the SIL values when comparing the accuracy of decomposition between surface and intramuscular recordings. In all cases, the SIL values for the HD-iEMG were higher than those from the HD-sEMG, and the difference increased with increasing contraction force.

D. Number of Motor Units and Accuracy of Decomposition as a Function of Channel Selection

Table II reports the mean and standard deviation of the number of motor units decomposed from the electrode configurations with fixed IED (refer to Fig. 2 **c**). The yields exhibited a negative correlation with IED, with a more marked impact of the number of motor units for higher contraction levels (only 1.8 motor units were decomposed at 70 %MVC level with 4 mm IED for S1, and no motor units were decomposed at that level for S2).

Figure 8 and Figure 9 present two key analyses at 30 %MVC. Figure 8 shows the mean and standard deviation of the number of decomposed motor units, while Figure 9 displays the mean and standard deviation of the SIL values for those units. These results were obtained from various random subsampling configurations (refer to Fig. 2 **d**). The data are organised by electrode, with channels divided into three subsets of 40 channels each. In addition, scatter points in the figures represent the mean yield (Fig. 8) and mean SIL (Fig. 9) for the fixed IED configuration. The analysis reveals a clear trend: as the number of channels increases, the number of decomposed motor units increases, and the SIL values generally improve. The SIL values show greater variability when fewer than 10 channels are used, consistent with the findings from Figure 7 **a**. Importantly, the number of motor units decomposed and their SIL values in the fixed IED configuration closely follow the trend observed in the random subsampling data, indicating that the number of channels,

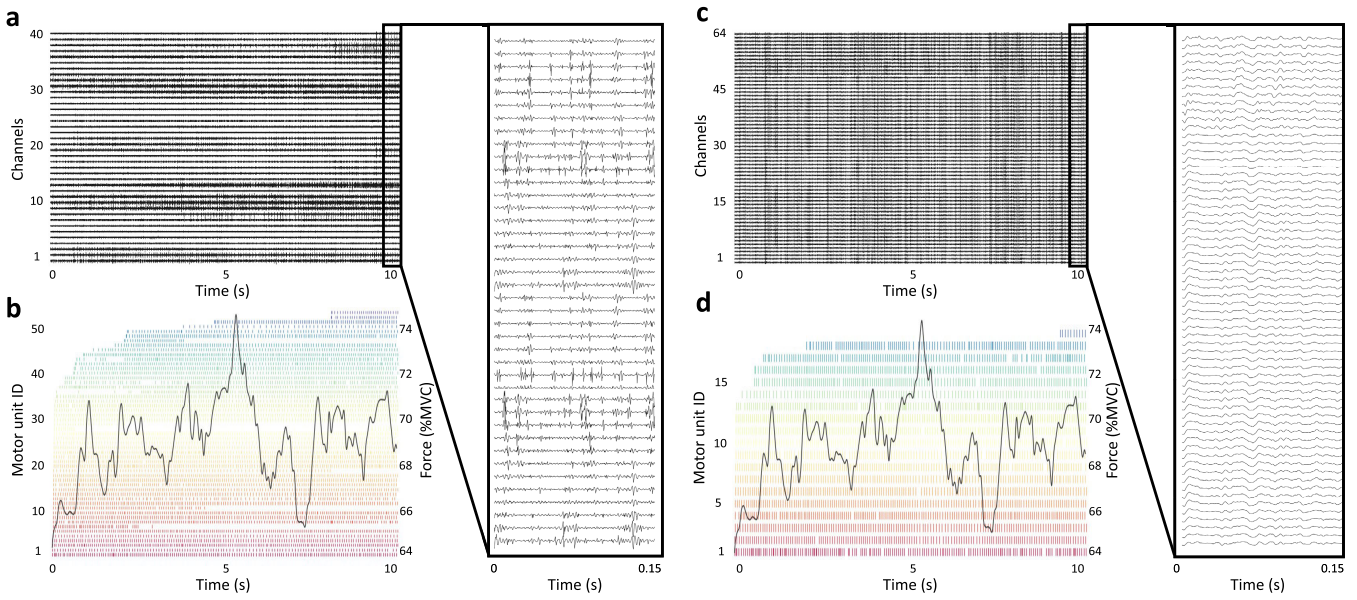

Fig. 5. Example data and respective raster plots. **a** HD-iEMG (40 channels, 10 seconds), with a 150 ms zoom-in on the data **b** Raster plot from the HD-iEMG (120 channels) **c** HD-sEMG (64 channels, 10 seconds), with a 150 ms seconds zoom-in on the data **d** Raster plot from the HD-sEMG (192 channels).

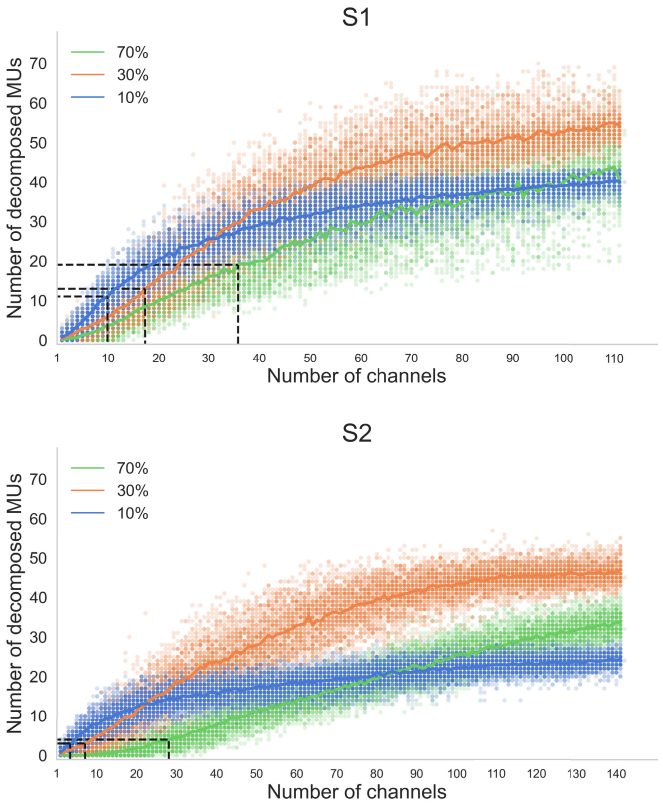

Fig. 6. Effect of the number of random channels (**a**) on the number of identified motor units at 10, 30, and 70 %MVC for S1 (top) and S2 (bottom) (**b**). Each point represents one of the 100 permutations for each channel count. The solid line indicates the mean yield of these permutations. Horizontal dashed lines show the motor unit yield from HD-sEMG decomposition, while vertical dashed lines denote the number of intramuscular channels needed to achieve the same yields.

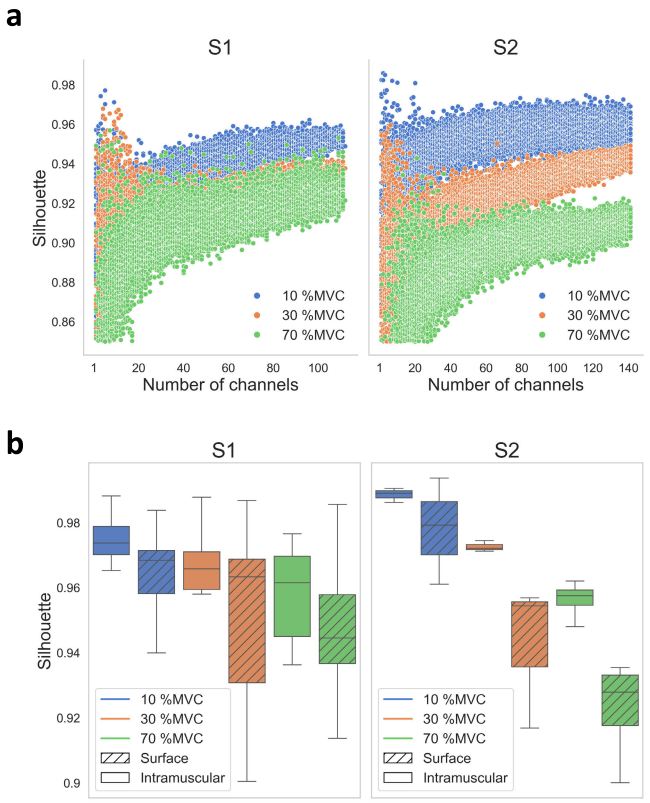

Fig. 7. Effect of channel number on the accuracy of decomposition. **a** Mean SIL value of each permutation run for the HD-iEMG, for the three force levels (10, 30, 70 %MVC) and the two subjects (S1, S2). **b** Distribution of SIL values for the intramuscular and surface EMGs, and for the three force levels (10, 30, 70 %MVC).

rather than their specific location in the muscle, is the primary factor driving decomposition performance. Note that this does not mean that all channel selections will lead to very similar number of decoded motor units. As commented in relation to Figure 6, there is a large variability of number of decoded motor units across permutations. Yet, on average, choosing

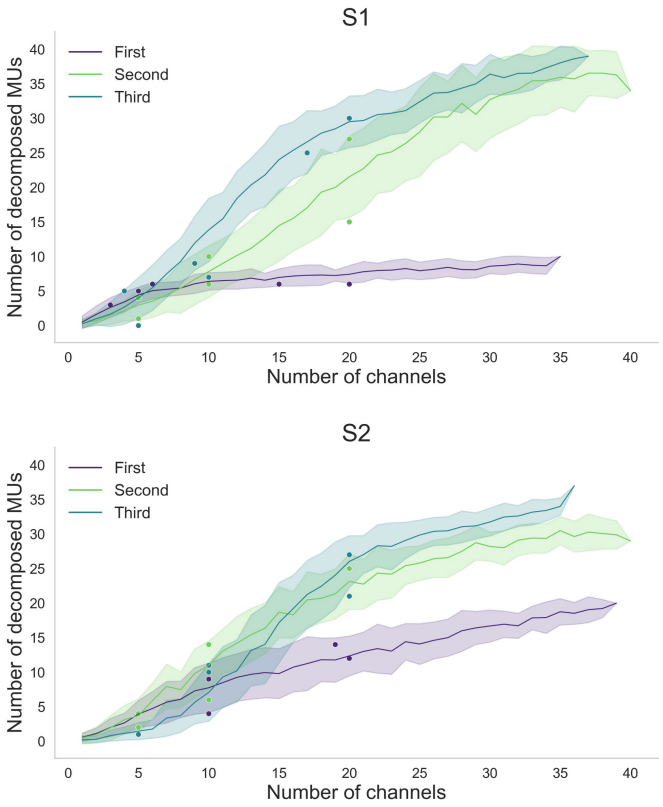

Fig. 8. Effect of the channel location on the number of decomposed motor units for each channel configuration. Results are reported for S1 and S2 at 30 %MVC, per electrode. The solid line indicates the average number of motor units decomposed from the random selection of channels. The shaded area represents the standard deviation. The scatter points represent the number of motor units decomposed from the fixed IED configurations.

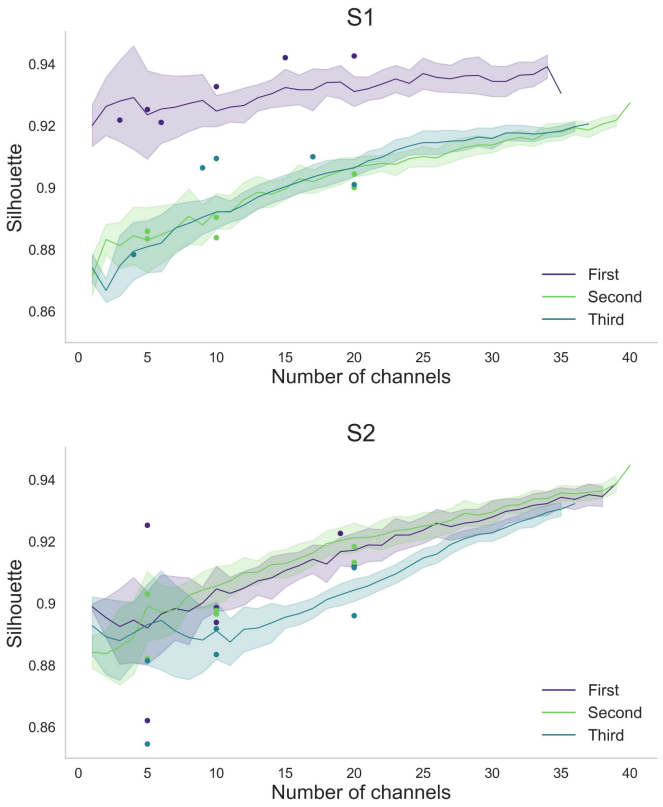

Fig. 9. Effect of the channel location on the mean SIL for each channel configuration. Results are reported for S1 and S2 at 30 %MVC, per electrode. The solid line indicates the average SIL of the units decomposed from the random selection of channels. The shaded area represents the standard deviation. The scatter points represent the mean SIL decomposed from the fixed IED configurations.

the channels randomly along the micro-electrode array led to similar results. Since it is not possible to determine the channel position along the array that leads to the best performance a priori, maximising the number of channels, rather than optimising their locations, has the largest effect on the number of decoded units.

The number of common units identified across the intramuscular micro-electrode array electrodes and their RoA is presented in Figure 10. The common units are low for S1 across electrodes. For S2, the numbers are generally low, except for 30 %MVC, where 18 units are shared between the first and second electrodes, and another set of 18 units is shared between the second and third electrodes.

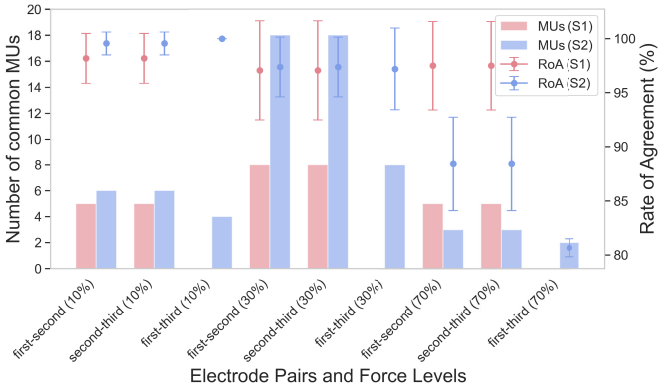

Fig. 10. Counts of common motor units across intramuscular electrodes for S1 and S2, and the three force levels. The error bars indicate the RoA (mean and std) between the common units.

IV. Discussion

This study systematically investigated the impact of parameters of HD-iEMG micro-electrode arrays on the number of identified motor units and the accuracy of their decomposition. This is the first study to record muscle activities using >140 electrode sites inside the muscle simultaneously.

The analysis of motor units extracted from both HD-iEMG and HD-sEMG recordings demonstrated physiologically consistent discharge rates (Fig. 3). The discharge rate distribution for the motor units identified with HD-sEMG was similar to that for motor units decomposed from HD-iEMG, particularly for subject S1. Therefore, despite the lower yield of decomposed units from HD-sEMG, the extracted population appeared to be representative of the broader motor unit pool. The motor units derived from the HD-iEMG showed the expected inverse relationship between recruitment threshold and discharge rate, with earlier-recruited units exhibiting higher firing frequencies compared to later-recruited units [23]. The recruitment pattern of the HD-iEMG motor units revealed predominantly uniform unit recruitment throughout the contractions, with the exception of 70 %MVC in subject S2, where early-recruited units were underrepresented in the

decomposition. This likely occurred because smaller action potentials from early-recruited units were masked by larger action potentials from later-recruited units. For subject S1, the recruitment-discharge rate relationship remained consistent between HD-iEMG and HD-sEMG recordings. However, the limited number of decomposed units from the HD-sEMG decomposed from subject S2 precluded meaningful analysis on the recruitment pattern.

Our findings show that increasing the number of channels results in the identification of a greater number of motor units, consistent with previous analogous research conducted with surface electrodes [26]. The result is not obvious since the channels were always selected within the same micro-electrode array and thus always covered the same portion of muscle section. Therefore, the only variable analysed was electrode density rather than different areas of muscle investigated. The increase in number of detected units with increasing number of channels may be partly due to the sampling of motor units with more channels but more likely it was determined by a better identification of separation filters with a greater electrode density.

Furthermore, we examined whether the selection of channel locations, given a fixed density, is critical for motor unit decomposition. The results indicated that the yields and accuracy from random channel subsampling closely matched those from fixed IED configurations on average. This indicates that the accuracy is not significantly impacted by whether the channels are selected randomly or arranged in a closely spaced configuration, as long as they are selected from the same array. This confirms that the density of channels is the most critical factor when optimising for the yield of MUs. Moreover, given the lack of convergence in the observed trends, using larger sets of channels with even shorter IEDs than in this study (i.e., $<$0.5 mm) could potentially lead to even better performance.

We also compared the results between HD-sEMG grids and HD-iEMG. The number of motor units decomposed from HD-sEMG was considerably lower than from HD-iEMG. Additionally, the results (in terms of yield and SIL) were variable across subjects at the surface level, while they were more consistent at the intramuscular level. Similar number of motor units were obtained with the two subjects in all conditions with HD-iEMG, indicating lower intra-subject variability compared to HD-sEMG. This higher variability in HD-sEMG is likely due to its greater sensitivity to subject-specific factors, such as volume conduction effects and electrode shifts [27], [28], [29]. The accuracy of decomposition was also lower in the HD-sEMG setting compared to the HD-iEMG (Fig. 7). This can be attributed to the superior quality of HD-iEMG recordings, which, due to their spatial selectivity, can record units in 6-8 channels. Intramuscular recordings thus result in a much greater temporal and spatial sparseness than surface recordings, and this is a significant factor in determining differences between the two methods.

In agreement with recent findings for surface recordings [26], our findings show that denser arrays allow better spatial sampling, which improves the identification of MUs, especially at higher force levels. The number of motor units plateaued at 10% and 30 %MVC in S1 (Fig. 6), but continued to rise at 70 %MVC. A similar trend was observed in S2. This suggests that increasing the density of recording points could be particularly advantageous for decomposing data acquired at higher force levels.

As shown in Figure 8, the number of channels, rather than their specific placement within the muscle, was the primary factor influencing the yield of decomposed motor units. Additionally, Figure 9 supports the claim that decomposition accuracy improves with increased channel count, as evidenced by consistent SIL trends across all electrodes and both subjects, with the exception of the first electrode in S1. This electrode deviated from the overall trend also in the motor unit yield. Indeed, unlike the other electrodes, it produced fewer decomposed motor units overall, which likely explains the differing SIL trend observed (Fig. 8).

The number of common surface/intramuscular units across modalities was very small, which can be attributed to the different regions of the muscle recorded with the surface and intramuscular electrodes. Additionally, the number of common units across intramuscular arrays was also low, except for S2 at 30 %MVC. The limited overlap of units across intramuscular electrodes is likely attributable to the high spatial selectivity of intramuscular recordings, which inherently reduces the likelihood of sampling the same muscle fibers from different electrode insertions. The higher number of common units for S2 at 30 %MVC may explain the slightly lower overall number of motor units found for S2 (refer to Table I). In the future, the ability to re-target electrodes after identifying common motor units across electrodes could facilitate the recording of unique MUs, thereby expanding the pool of identified motor units by multiple arrays. The TA comprises roughly 445 motor units [30]. Given the limited overlap of motor units identified between HD-sEMG and HD-iEMG (as well as among different intramuscular electrodes), combining data from both modalities could significantly expand the pool of motor neurons detected, allowing for a more comprehensive estimate of the neural drive to the muscles.

Future technologies should consider leveraging the advantages of HD-iEMG for studying the neuromechanics of movement and for neural interfacing. The greater consistency in results, along with the higher number of decomposed motor units and improved decomposition accuracy with respect to HD-sEMG, make HD-iEMG a promising tool for this research. Further advancements in intramuscular technologies could benefit from increasing both the number and the density of channels within the array. While our focus in this study was on a large muscle like the TA, which provides access to a large pool of motor units, further studies are necessary to determine whether these findings extend to muscles with different anatomical characteristics, such as differences in muscle size, fiber pinnation angles, and distribution of end-of-fiber regions.

Acknowledgment

The authors would like to thank Dr. Silvia Muceli, Dr. Aritra Kundu, Dr. Simon Avrillon, and Dr. Alejandro Pascual Valdunciel for their help during the data collection.

REFERENCES

[1] K. D. Bergmeister et al., "Peripheral nerve transfers change target muscle structure and function," *Sci. Adv.*, vol. 5, no. 1, Jan. 2019, Art. no. eaau2956.

[2] D. Sussillo, P. Kaifosh, and T. R. Reardon, "A generic noninvasive neuromotor interface for human-computer interaction," *bioRxiv*, Feb. 2024.

[3] E. D. Adrian and D. W. Bronk, "The discharge of impulses in motor nerve fibres: Part II. The frequency of discharge in reflex and voluntary contractions," *J. Physiol.*, vol. 67, no. 2, pp. 151–159, Mar. 1929.

[4] S. Muceli, W. Poppendieck, A. Holobar, S. Gandevia, D. Liebetanz, and D. Farina, "Blind identification of the spinal cord output in humans with high-density electrode arrays implanted in muscles," *Sci. Adv.*, vol. 8, no. 46, Nov. 2022, Art. no. eabo5040.

[5] D. Farina and S. Gandevia, "The neural control of movement: A century of in vivo motor unit recordings is the legacy of Adrian and Bronk," *J. Physiol.*, vol. 602, no. 2, pp. 281–295, Jan. 2024.

[6] D. Farina and R. M. Enoka, "Evolution of surface electromyography: From muscle electrophysiology towards neural recording and interfacing," *J. Electromyogr. Kinesiol.*, vol. 71, Aug. 2023, Art. no. 102796.

[7] M. Zheng, M. S. Crouch, and M. S. Eggleston, "Surface electromyography as a natural human–machine interface: A review," *IEEE Sensors J.*, vol. 22, no. 10, pp. 9198–9214, May 2022.

[8] S. Muceli et al., "Accurate and representative decoding of the neural drive to muscles in humans with multi-channel intramuscular thin-film electrodes," *J. Physiol.*, vol. 593, no. 17, pp. 3789–3804, Sep. 2015.

[9] D. Farina, F. Negro, S. Muceli, and R. M. Enoka, "Principles of motor unit physiology evolve with advances in technology," *Physiology*, vol. 31, no. 2, pp. 83–94, Mar. 2016.

[10] L. Mesin, R. Merletti, and A. Rainoldi, "Surface EMG: The issue of electrode location," *J. Electromyogr. Kinesiol.*, vol. 19, no. 5, pp. 719–726, Oct. 2009.

[11] K. G. Keenan, D. Farina, K. S. Maluf, R. Merletti, and R. M. Enoka, "Influence of amplitude cancellation on the simulated surface electromyogram," *J. Appl. Physiol.*, vol. 98, no. 1, pp. 120–131, Jan. 2005.

[12] D. Farina, R. Merletti, B. Indino, M. Nazzaro, and M. Pozzo, "Surface EMG crosstalk between knee extensor muscles: Experimental and model results," *Muscle Nerve*, vol. 26, no. 5, pp. 681–695, 2002.

[13] D. Stashuk, "EMG signal decomposition: How can it be accomplished and used?" *J. Electromyogr. Kinesiol.*, vol. 11, no. 3, pp. 151–173, Jun. 2001.

[14] P. Zhou and W. Z. Rymer, "MUAP number estimates in surface EMG: Template-matching methods and their performance boundaries," *Ann. Biomed. Eng.*, vol. 32, no. 7, pp. 1007–1015, Jul. 2004.

[15] B. U. Kleine, J. P. van Dijk, B. G. Lapatki, M. J. Zwarts, and D. F. Stegeman, "Using two-dimensional spatial information in decomposition of surface EMG signals," *J. Electromyogr. Kinesiol.*, vol. 17, no. 5, pp. 535–548, Oct. 2007.

[16] A. Holobar and D. Zazula, "Multichannel blind source separation using convolution kernel compensation," *IEEE Trans. Signal Process.*, vol. 55, no. 9, pp. 4487–4496, Sep. 2007.

[17] Y. Ning, X. Zhu, S. Zhu, and Y. Zhang, "Surface EMG decomposition based on K-means clustering and convolution kernel compensation," *IEEE J. Biomed. Health Informat.*, vol. 19, no. 2, pp. 471–477, Mar. 2015.

[18] A. Holobar and D. Zazula, "Gradient convolution kernel compensation applied to surface electromyograms," in *Proc. Int. Conf. Independ. Compon. Anal. Signal Separat.* Berlin, Germany: Springer, 2007, pp. 617–624.

[19] A. Holobar, V. Glaser, J. A. Gallego, J. L. Dideriksen, and D. Farina, "Non-invasive characterization of motor unit behaviour in pathological tremor," *J. Neural Eng.*, vol. 9, no. 5, Oct. 2012, Art. no. 056011.

[20] F. Negro, S. Muceli, A. M. Castronovo, A. Holobar, and D. Farina, "Multi-channel intramuscular and surface EMG decomposition by convolutive blind source separation," *J. Neural Eng.*, vol. 13, no. 2, Apr. 2016, Art. no. 026027.

[21] A. Grison, A. K. Clarke, S. Muceli, J. Ibáñez, A. Kundu, and D. Farina, "A particle swarm optimised independence estimator for blind source separation of neurophysiological time series," *IEEE Trans. Biomed. Eng.*, vol. 72, no. 1, pp. 227–237, Jan. 2025.

[22] E. Martinez-Valdes, F. Negro, C. M. Laine, D. Falla, F. Mayer, and D. Farina, "Tracking motor units longitudinally across experimental sessions with high-density surface electromyography," *J. Physiol.*, vol. 595, no. 5, pp. 1479–1496, Mar. 2017.

[23] C. J. De Luca and E. C. Hostage, "Relationship between firing rate and recruitment threshold of motoneurons in voluntary isometric contractions," *J. Neurophysiol.*, vol. 104, no. 2, pp. 1034–1046, Aug. 2010.

[24] B. Mambrito and C. J. De Luca, "A technique for the detection, decomposition and analysis of the EMG signal," *Electroencephalogr. Clin. Neurophysiol.*, vol. 58, no. 2, pp. 175–188, Aug. 1984.

[25] M. Gazzoni, D. Farina, and R. Merletti, "A new method for the extraction and classification of single motor unit action potentials from surface EMG signals," *J. Neurosci. Methods*, vol. 136, no. 2, pp. 165–177, Jul. 2004.

[26] A. H. Caillet et al., "Larger and denser: An optimal design for surface grids of EMG electrodes to identify greater and more representative samples of motor units," *Eneuro*, vol. 10, no. 9, Sep. 2023.

[27] R. C. Araujo, M. Duarte, and A. C. Amadio, "On the inter-and intra-subject variability of the electromyographic signal in isometric contractions," *Electromyogr. Clin. Neurophysiol.*, vol. 40, no. 4, pp. 225–230, 2000.

[28] A. H. Oskouei, M. G. Paulin, and A. B. Carman, "Intra-session and inter-day reliability of forearm surface EMG during varying hand grip forces," *J. Electromyogr. Kinesiol.*, vol. 23, no. 1, pp. 216–222, Feb. 2013.

[29] F. Hug, "Can muscle coordination be precisely studied by surface electromyography?" *J. Electromyogr. Kinesiol.*, vol. 21, no. 1, pp. 1–12, Feb. 2011.

[30] R. M. Enoka and A. J. Fuglevand, "Motor unit physiology: Some unresolved issues," *Muscle Nerve*, vol. 24, no. 1, pp. 4–17, 2001.